FULL LENGTH PAPER

EFFECT OF TURBULENCE MODEL AND SPRAY PARAMETERS ON KEROSENE FUELLED SCRAMJET COMBUSTOR

Malsur Dharavath; P. Manna; Debasis Chakraborty
Defence Research and Development Laboratory (DRDL)
Kanchanbagh Post, Hyderabad-500 058
Email : debasis_cfd@drdl.drdo.in; debasis_drdl@yahoo.co.in

Abstract

Numerical simulations are carried out for scramjet combustor with fuel injector struts to evaluate its performance for ground test conditions. Simulations were carried out for non-reacting and reacting flow with equivalence ratio of 1.0. CFD predicted top wall pressure compared reasonably well with experimental results except the upstream (ahead of the fuel injection) regions of the combustor where CFD has predicted higher values compared to the measured values. Effect of various spray distribution and turbulence models on wall pressure distribution and performance of the combustor studied. SST-kω turbulence model has predicted close to experimental data at upstream of combustion compared to k-ε, k-ω turbulence models. The net calculated combustion efficiency and achieved thrust at exit of combustor are 3% and 2.7% respectively higher in k-ω compared to SST-kω though total pressure recovery in all three cases are almost similar.

Keywords: *Scramjet combustor; CFD; Spray parameter; Turbulence models*

Introduction

Use of air-breathing engines is considered to be an alternative to rocket-based space vehicles for trans-atmospheric flight for high speed applications. Design and development of a hypersonic airbreathing cruise vehicle largely depends on the proper choice of propulsion system. This type of vehicle would use supersonic combustion as propulsion device. Both hydrogen and hydrocarbon fuels are considered depending on applications and various ranges of flight Mach number [1]. Although, hydrogen has attractive features in terms of specific impulse, ignition characteristics, etc., liquid hydrocarbon fuel is preferred for volume limited missile applications in the lower hypersonic region (M < 8). Because these applications impose volume constraints, a strong motivation exists for the development of a hydrocarbon-fuelled airframe integrated scramjet. Since residence time of the fuel is very less, atomization, vaporization, mixing and combustion are some of the major technical and scientific problems in the realization of liquid hydrocarbon fuelled scramjet combustor. A deeper penetration of fuel into a supersonic air stream enhances better mixing and thus performs efficient combustion inside the combustor. The penetration of liquid jet is studied extensively [2] for varying dynamic pressure ratios of two streams and different droplet sizes. In the flight region of Mach 6.0 - 7.0, a typical penetration depth of the fuel jet of about 10 to 15 mm is reported for a practical scramjet combustor. Though, studies of supersonic combustion with hydrocarbon fuels are performed over the past 30 years, only a limited design data base (Northam et. al. [3] and Waltrup [4]) is available in open literature.

Various injection strategies including wall injection [5, 6, 7, 8], ramp cavity [9, 10], strut [11, 12], pylons [13] etc. were tried for both hydrocarbon and hydrogen fuelled scramjet combustor. When the fuel is injected from the combustor wall or ramp cavity, reaction occurs only in a small fraction of the flow field adjacent to the wall. Hence, only a small zone of the flow field participates in the heat release process. For a practical flight sized combustor, with wall injections, core of the flow does not participate in combustion process due to non-availability of fuel resulting in inefficient combustion. Also, due to the occurring of reaction close to the surface, combustor walls experience excessive thermal loads and the walls are made

Paper Code : V67 N3/879-2015. Manuscript received on 30 Sep 2014. Reviewed, revised and accepted as a Full Length Contributed Paper on 20 Mar 2015

thicker to withstand the high thermal load. The problem of lateral fuel transport in the air stream can be circumvented by injecting the fuel in the core region of the flow by means of struts [11, 12] and or pylons [13]. The oblique shocks generated from the struts also augment the mixing which is very much needed in high speed propulsion devices. Manna et. al. [12] have numerically explored the effect of the combustor inlet Mach number and total pressure on the flow development in the kerosene fuelled scramjet combustor. It was shown that higher combustor entry Mach number and distributed fuel injection are required to obtain predominant supersonic flow and avoid thermal choking. The presence of fuel injection struts makes the flow fully three-dimensional, causes significant flow blockage and affects the mixing and combustion pattern in the scramjet combustor.

The effect of new strut geometry in the mixing and combustion process of a flight worthy scramjet combustor is numerically explored in this present work. Paneerselvam et. al. [14] presented a typical cruise hypersonic air-breathing mission where it was intended to demonstrate the autonomous functioning of airframe integrated scramjet engine in cruise mode for 20 seconds with earth storable kerosene fuel at free stream Mach number 6.5 and altitudes of 32.5 km. For operational convenience, ground launch option is adopted for the proposed mission. The cruise vehicle is housed above a first stage of a launch vehicle and carried to the desired altitude before injecting into the atmosphere. A rectangular geometry with seven fuel injection stuts with 120 injectors (0.5 mm diameter) was considered for the geometry. Different divergence angles were given to top wall to make the cross-section varying along the length of the combustor. Further details of the combustor are available in Ref.[14-16]. Number of ground test in connected pipe mode tests [15,16] and detailed three dimensional reacting CFD numerical simulations [17] were carried out to finalize the number of struts, their positions and fuel injection locations to have benign thermal environment and optimum performance of the flight sized engine.

While realising the airframe integrated scramjet vehicle, the weight of various subsystems is increased significantly and the free stream Mach number for scramjet operating condition has reduced to 6.0 from 6.5 and also the free stream total temperature reduced to 1723 K from 1970 K. This change of free stream condition has increased the nonuniformity of flow profiles at combustor entrance. All these changes resulted in non-ignition/intermittent ignition of kerosene in the combustor and use of auxiliary ignition devices (pilot hydrogen/ethylene) could not solve the ignition problem satisfactorily in the existing design. To circumvent the ignition problem, a new design of strut with wide base is adopted [18] to have a larger recirculation zone of kerosene fuel in the strut base.

The nonreacting and reacting flow field of the kerosene fuelled scramjet combustor with new wide based strut geometry is explored numerically in this paper by solving three dimensional Navier Stokes equations alongwith two equation turbulence models, infinitely fast rate chemical kinetics and eddy dissipation based combustion model. Thermochemical variables are analysed to get a better insight of mixing and combustion process inside the combustor and computed wall pressures are compared with experimental data for the new geometry. The performance of various turbulence models in predicting reacting flow in practical scramjet combustor is not studied adequately in open literature. In the present work, we assessed three different two equation turbulence models for their predictive capabilities of turbulent reacting flow in a flight sized kerosene fuelled scramjet combustor. Parametric studies are also conducted to study the effect of spray parameters on scramjet wall pressures.

Scramjet Combustor - Geometry and Experimental Condition

The full scale proof hardware of scramjet combustor with fuel injector struts was directly connected to a blow-down type high enthalpy test facility. A vitiated air heater (hydrogen burner with make-up oxygen supply) was used to obtain high enthalpy airflow for equivalent flight condition of total temperature and total enthalpy of 1650-1750 K and 1.55-1.65 MJ/kg respectively. Test gas was accelerated through a contoured convergent-divergent nozzle to Mach 2.2 at combustor entry.

The two module scramjet combustor with fuel injector system of 8-strut arrangement is considered for numerical analysis. Schematic diagram of the scramjet combustor with a part of the facility nozzle is shown in Fig.1a. The combustor dimensions were non-dimensionalised with combustor entry height (h). The length of the facility nozzle and combustor is $5h$ and $22h$ respectively, while width of the combustor including facility nozzle remains the same and is $6h$ throughout the length. The combustor has four sections. The 1st section has a constant area with

a length h, followed by 1° divergent (2nd section) for $2h$ length, 4° divergent (3rd section) for $8h$ length and finally 7.5° divergent (4th section) of $10h$ length. To have modular structure, a middle wall with a thickness of $0.2h$ is placed at a distance of $3h$ downstream from combustor entry in the middle of the combustor which makes combustor into two modules. The width of the combustor is sufficiently large and the middle wall joins both top and bottom wall in the middle and thus provides support for both the walls. Also the leading edge of the middle wall compresses the incoming air flow, generating various shocks structures which produce higher static pressure and temperature at the regions ahead of the first struts. This creates a better environment for initiation of ignition of the fuel comes out from the first struts. Four struts are provided in each module in such a manner that one module is the mirror image of the other about the middle wall. The struts are straight and cross section remains constant along the height of the combustor as shown in Fig.1b. The cross sectional length and the base width of the struts are $0.7h$ mm and $0.3h$ respectively. First strut is placed near to the middle wall while 4th strut near to the side wall.

Computational Methodology

Three-dimensional Reynolds Averaged Navier Stokes (RANS) equations along with species and turbulence transport equations are solved using computational flow code CFX [19] to study the high speed reacting flow of HSTDV-CV scramjet combustor. The CFX-code is an integrated software system capable of solving diverse and complex multidimensional fluid flow problems. The code is fully implicit, finite volume method with finite element based discretization of geometry. The method retains much of the geometric flexibility of finite element methods as well as the important conservation properties of the finite volume method. It utilizes numerical upwind schemes to ensure global convergence of mass, momentum, energy and species. It implements a general non-orthogonal, structured and unstructured, boundary fitted grids. To circumvent the initial numerical transient, the discretization of the convective terms are done by first order upwind difference scheme till few time steps initially and subsequently, the convective terms are discretized through 2nd order scheme to capture the flow features more accurately. The set of equations solved by CFX are the unsteady RANS equations in their conservation form. The turbulence was solved using k-ε [20], k-ω [21] or SST-kω [22] models along with wall functions. The details are given in following section.

Governing Equations

The appropriate system of governing equations of mass, momentum, energy, turbulent and species transport equations of an unsteady compressible gas flow may be written as:

Conservation of Mass equation:

$$\frac{\partial \rho}{\partial t} + \frac{\partial}{\partial x_k}(\rho u_k) = 0 \quad k = 1, 2, 3 \tag{1}$$

Conservation of Momentum equation:

$$\frac{\partial}{\partial t}(\rho u_i) + \frac{\partial}{\partial x_k}(\rho u_i u_k) + \frac{\partial P}{\partial x_i} = \frac{\partial(\tau_{ik})}{\partial x_k}, \quad i, k = 1, 2, 3 \tag{2}$$

Conservation of Energy equation:

$$\frac{\partial}{\partial t}(\rho H) + \frac{\partial}{\partial x_k}(\rho u_k H) = -\frac{\partial}{\partial x_k}(u_j \tau_{jk}) + \frac{\partial q_k}{\partial x_k}, \quad j, k = 1, 2, 3 \tag{3}$$

Turbulence Transport Equations

k-ε Turbulence Model

Turbulent Kinetic Energy (k) equation:

$$\frac{\partial}{\partial t}(\rho k) + \frac{\partial}{\partial x_k}(\rho u_k k) = \frac{\partial}{\partial x_k}\left(\left(\frac{\mu_l}{\mathrm{Pr}} + \frac{\mu_t}{\sigma_k}\right)\frac{\partial k}{\partial x_k}\right) + S_k \tag{4}$$

Turbulent Eddy Dissipation (ε) equation:

$$\frac{\partial}{\partial t}(\rho \varepsilon) + \frac{\partial}{\partial x_k}(\rho u_k \varepsilon) = \frac{\partial}{\partial x_k}\left(\left(\frac{\mu_l}{\mathrm{Pr}} + \frac{\mu_t}{\sigma_\varepsilon}\right)\frac{\partial \varepsilon}{\partial x_k}\right) + S_\varepsilon \tag{5}$$

Where, ρ, u_i, p, H are the density, velocity components, pressure and total energy respectively and $\mu = \mu_l + \mu_t$ is the total viscosity; μ_l, μ_t being the laminar and turbulent viscosity and Pr is the Prandtl number. The source terms S_k and S_ε of the k and ε equation are defined as

$$S_k = \tau_{ik}\frac{\partial u_i}{\partial x_k} - \rho\varepsilon \text{ and } S_\varepsilon = C_{\varepsilon 1}\tau_{ik}\frac{\partial u_i}{\partial x_k} - C_{\varepsilon 2}\frac{\rho \varepsilon^2}{k}$$

Where turbulent shear stress is defined as

$$\tau_{ik} = \mu_t \left(\frac{\partial u_i}{\partial x_k} + \frac{\partial u_k}{\partial x_i} \right) \quad (6)$$

Laminar viscosity (μ_l) is calculated from Sutherland law as

$$\mu_l = \mu_{ref} \left(\frac{T}{T_{ref}} \right)^{3/2} \left(\frac{T_{ref} + S}{T + S} \right) \quad (7)$$

Where, T is the temperature and μ_{ref}, T_{ref} and S are known coefficient. The turbulent viscosity μ_t is calculated as,

$$\mu_t = C_\mu \frac{\rho k^2}{\varepsilon} \quad (8)$$

The coefficients involved in the calculation of turbulent viscosity (μ_t) are taken as

$$c_\mu = 0.09, \qquad C_{\varepsilon 1} = 1.44, \qquad C_{\varepsilon 2} = 1.92$$

$$\sigma_\kappa = 1.0, \qquad \sigma_\varepsilon = 1.3, \qquad \sigma_c = 0.9$$

The heat flux q_k is calculated as $q_k = -\lambda \frac{\partial T}{\partial x_k}$, λ is the thermal conductivity.

k-ω Turbulence Model

In this model, turbulent viscosity is calculated as function of k and ω [21].

$$\mu_t = f \left(\frac{\rho k}{\omega} \right) \quad (9)$$

Turbulent Kinetic energy (k) equation:

$$\frac{\partial}{\partial t}(\rho k) + \frac{\partial}{\partial x_i}(\rho k u_i) = \frac{\partial}{\partial x_j} \left(\Gamma_k \frac{\partial k}{\partial x_j} \right) + G_k - Y_k \quad (10)$$

Specific Dissipation Rate (ω) equation:

$$\frac{\partial}{\partial t}(\rho \omega) + \frac{\partial}{\partial x_i}(\rho \omega u_i) = \frac{\partial}{\partial x_j} \left(\Gamma_\omega \frac{\partial \omega}{\partial x_j} \right) + G_\omega - Y_\omega \quad (11)$$

Where, G_k is turbulence production due to viscous and buoyancy forces,

$Y_k = \beta^1 \rho k w$, $\Gamma_k = \mu + \frac{\mu_t}{\sigma_k}$, $G_w = \alpha \frac{\omega}{k} G_k$, $Y_w = \beta \rho w^2$

and $\Gamma_w = \mu + \frac{\mu_t}{\sigma_w}$ of the k and ω equations respectively.

Where $\beta^1 = 0.09$, $\alpha = 5/9$, $\beta = 0.075$, and $\sigma_k = \sigma_w = 2$.

SST - *k*ω Turbulence Model

To retain the robust and accurate formulation of Wilcox's k- ω model in the near wall region, and take advantage of the free stream independence of the k- ε model in the outer part of the boundary layer, Menter [22] blended both the models through a switching function. k- ε model was transformed into Wilcox's k- ω formulation and was multiplied by $(1\text{-}F_1)$ and added to original k- ω model multiplied by F_1. The blending function F_1 will be one in the near wall region and zero away from the surface. In the second step, the definition of eddy viscosity (μ_t) was modified in the following way to account for the transport of the principal turbulent shear stress ($\tau = -\rho \overline{u' v'}$)

$$v_t = \frac{a_1 k}{\max(a_1 \omega ; \Omega F_2)} \quad (12)$$

where v_t (is kinematic viscosity) $= \mu_t / \rho$ and F_2 is a blending function similar to F_1, which restricts the limiter to the wall boundary layer. Ω is an invariant measure of the strain rate. Their formulation is based on the distance to the nearest surface and on the flow variables.

$$F_2 = \tan h (ar g_2^4) \quad (13)$$

The argument is defined as

$$ar g_2 = \min \left[\max \left\{ \frac{\sqrt{k}}{0.09 \omega y'}, \frac{500 v}{y^2 \omega} \right\}, \frac{4 \rho \sigma_{\omega 2} k}{y^2 CD_{k\omega}} \right] \quad (14)$$

Where y is the distance to the wall and $CD_{k\omega}$ the positive portion of the cross-diffusion terms expressed as

$$CD_{k\omega} = \max \left[2 \rho \sigma_{\omega 2} \frac{1}{\omega} \frac{\partial k}{\partial x_j} \frac{\partial \omega}{\partial x_j}, 10^{-20} \right] \quad (15)$$

Where, y is the distance to the nearest wall and v is the kinematic viscosity.

Species Transport Equation

Conservation of Species Mass Fraction (Y_I):

$$\frac{\partial}{\partial t}(\rho Y_I) + \frac{\partial}{\partial x_k}(\rho u_k Y_I) = \frac{\partial}{\partial x_k}\left(\left(\frac{\mu_l}{\mathrm{Pr}} + \frac{\mu_t}{\sigma_c}\right)\frac{\partial Y_I}{\partial x_k}\right) + S_I \qquad (16)$$

Where the source term S_I is due to the chemical reaction rate involving species component I, and Y_I is the mass fraction of I^{th} species. The chemical reactions can be described in terms of k elementary reactions involving N_C components that can be written as:

$$\sum_{I=A,B,C,\ldots}^{N_C} v_{kI}' I \quad \leftrightarrow \quad \sum_{I=A,B,C,\ldots}^{N_C} v_{kI}' I \qquad (17)$$

Where, v_{kI} is the stiochiometric coefficient for species component I in the elementary reaction k. The rate of production/consumption, S_I, for species component I can be computed as the sum of the rate of progress for all the elementary reactions in which component I participates:

$$S_I = M_{wI} \sum_{k=1}^{k} (v_{kI}' - v_{kI}') R_k \qquad (18)$$

Where, M_{wI} is molecular weight of species component I and R_k is the elementary reaction rate of progress for reaction, which can be calculated using combustion model.

Thermodynamic Model

A thermally perfect gas is assumed in the present study and consequently, the specific heats for all species are function of temperature only. The specific heats are calculated using a fourth order polynomial at the internal of fluid temperature 300 K - 5000 K. In each interval, the same form for the polynomials is used but different coefficients can be used.

$$\frac{C_{pi}}{R} = A_i + B_i T + C_i T^2 + D_i T^3 + E_i T^4 \qquad (19)$$

Where, A_i, B_i, C_i, and E_i are curvefit constants [19] and T is the fluid static temperature. C_{pi} is linearly extrapolated when the fluid temperature T < 300 K or T > 5000 K. Then, the static enthalpy h, is calculated as $h = \sum_{i=1}^{n} Y_i h_i(T)$ and the static enthalpy of each species, $h_i(T)$, is

$$h_i(T) = \Delta h_{fl}^o + \int_{T^o}^{T} C_{pi}(T)\, dT \qquad (20)$$

where, Δh_{fl}^o is the standard heat of formation of species I, defined as the heat evolved when one mole of substance is formed from its elements in their respective standard states at 298.15 K and 1.0 atmosphere. The fluid temperature is calculated based on the solution of the fluid enthalpy using a Newton's iteration method for finding the roots of the polynomials. An equation of state of the following form for a multi-component is used to calculate fluid density $\rho = P/(RT/W_m)$, where mixture molecular weight (W_m) is obtained by the following equation, $W_m = \left(\sum_{i=1}^{n} (Y_i/W_i)\right)^{-1}$ and R is the universal gas constant.

The Gibbs free energy is required to determine the equilibrium constants for the combined eddy dissipation and finite rate chemistry models. It is obtained for a constant pressure process by

$$\frac{g_i}{R} = A_i(T - \ln T) - \frac{B_i}{2}T^2 - \frac{C_i}{6}T^3 - \frac{D_i}{12}T^4 - \frac{E_i}{20}T^5 + F_i - G_i T \qquad (21)$$

Where, A_i, B_i, C_i, D_i, E_i, F_i and G_i are an additional curvefit constants [19].

Combustion Modeling

For combustion, the eddy dissipation combustion model is used for its simplicity and robust performance in predicting reactive flows. The eddy dissipation model is based on the concept that chemical reaction is fast relative to the transport process in the flow. When reactants mix at the molecular level they instantaneously form products. The model assumes that the reaction rate may be related directly to the time required to mix reactants at molecular level. In turbulent flows, this mixing time is dictated by the eddy properties and therefore the burning rate is proportional to the rate at which turbulent kinetic energy is dissipated i.e., reaction rate is propotional to ε/k, where k is the turbulent kinetic energy and ε is its rate of dissipa-

tion. The single step chemistry of the combustion reaction is represented on a molar basis by:

$$C_{12}H_{23} + 17.75\,O_2 = 12\,CO_2 + 11.5\,H_2O \qquad (22)$$

The mixing rate, determined from the Eddy dissipation Model (EDM), is given as

$$R_k = -A_{ebu}\,\bar{\rho}\,\frac{\varepsilon}{k}\,\min\left\{Y_f, \frac{Y_o}{r_s}, B_{ebu}\,\frac{Y_p}{1+v_s}\right\} \qquad (23)$$

where, Y_f, Y_o and Y_p are the mass fractions of fuel, oxidizer and products respectively, A_{ebu} and B_{ebu} are the model constants and v_s is the stiochometric ratio.

Rosin-Rammler Distribution

The different sizes of the liquid kerosene fuel drops are commonly described in Rosin-Rammler type distribution [23] and is expressed as,

$$R = 1 - \exp^{-(\frac{d_o}{d_e})^{\gamma}} \qquad (24)$$

Where, R is the fraction of the total mass contained in drops of diameter below d_o, d_e is a measure of the fitness and is equal to d_o at which $R = (1 - \frac{1}{e})$ or 0.632. γ is the spray parameter, which is a measure of size dispersion. In Rosin-Rammler distribution to sprays, it is possible to describe the drop size distribution in terms of the two parameters d_e and γ. The exponent γ provides a measure of the spread of drop sizes. The higher the value of γ, the more uniform is the spray. If the value of γ is infinite, all the drops in the spray are of same size. Typically, for liquid kerosene fuel sprays the value of γ lies in between 1.5 to 4.0.The spray parameters for different equivalence ratios are obtained from Ref. 24 and are tabulated in Table-1. In the present study, the case corresponding to equivalence ratio1 is considered and simulations are carried out for four cases of spray parameter values (γ) as shown in Table-2.

Results and Discussion

Taking the advantage of the symmetry of the geometry, only half of geometry (i.e. Module-2 as shown in Fig.1a) along width of the combustor is chosen for numerical simulations to reduce the computational time. The computational domain along with the facility nozzle and the combustor is shown in Fig.2. In the simulation, X-axis is taken along the flow direction (length of combustor), while, Y and Z-axis are chosen along the height and width of the combustor respectively, with the origin being placed at the intersect point between symmetry and bottom wall at combustor entry. Each strut contains nine injection holes on either side. All the injection holes have approximately the same size with a diameter of 0.5 mm. The schematic picture of strut-4 (zoomed view) showing the location of injection holes is also presented in Fig.2. Liquid kerosene ($C_{12}H_{23}$) is injected through 72 injection points provided in the 4 struts. The inlet condition as achieved in ground test at facility nozzle entry plane corresponds to the flight condition of Mach 6.0 at 31 km

Table-1 : Spray Parameters for Different Equivalence Ratio

Cases	Equivalence Ratio (φ)	SMD (μm)	Injection Velocity (m/s)	Rosin Rammler Parameters	
				d_e (μm)	γ
1	1.0	11.58	48.75	31.3	1.5
2	0.9	16.43	43.64	44.0	1.5
3	0.8	19.78	38.52	53.0	1.5
4	0.7	24.49	33.37	65.6	1.5
5	0.6	31.46	28.21	84.3	1.5

Table-2 : Rosin - Rammler d_e and γ

Cases	γ	SMD /d_e	Equiv. Ratio (ϕ) = 1.0	
			d_e (μm)	SMD (μm)
1	1.5	0.36971	31.31	11.58
2	2.0	0.56418	20.52	11.58
3	3.0	0.73848	15.68	11.58
4	4.0	0.81613	14.90	11.58

altitude. Kerosene liquid fuel injection with an equivalence ratio (ϕ) of 1.0 has been considered for numerical simulations.

Structured grids (hexahedral) are made using ICEM-CFD [25] for the complete computational domain. Since the geometry is very complex because of the presence of struts, middle wall and varying cross sectional area, it is divided into 520 blocks and grid were generated ensuring better quality (orthogonality, aspect ratio and skewness) and connectivity between the blocks. Total 2.6 million (396 x 65 x 101) grids were generated for the entire computational domain. The typical grid distribution for computational domain in *X-Y* plane at Z/h = 1.6 and *X-Z* plane at Y/h = 0.5 are shown in Fig.3. The grids are fine near the leading edge and trailing regions of the struts and near-wall regions, while relatively coarser grids are provided in the remaining portion of the nozzle and combustor. Average y^+ ~ 5 has been obtained for nozzle, combustor and struts walls. All the flow properties are kept constant in the entry plane of facility nozzle. No slip and adiabatic wall conditions are specified for all walls. The supersonic outflow boundary condition has been applied at the exit of the combustor. Log-normalized maximum residue of four order less for various flow variables and global mass, momentum, and energy imbalance less than 0.1% between outlet and inlet of the computational domain have been considered as the convergence criteria.

Numerical simulations carried out to study the flow characteristics of the combustor are summarized as follows:

i) Non-reacting Flow Simulation

a) Without fuel injection
b) with fuel injection

ii) Reacting flow simulations : Baseline simulation with k-ε model and γ = 1.5

a) Effect of spray parameter
b) Effect of turbulence model

Nonreacting Flow Simulation Results

Without Fuel Injection

The static pressure, Mach number and static temperature distribution and numerical schliren at mid-height of combustor entry plane (i.e. Y/h = 0.5) are shown in Fig.4. Simulations captured all the essential flow futures, i.e. oblique shocks generated due to middle wall and struts leading edge, expansion waves due to struts trailing edge and base and reflection shock generated due to side wall of combustor as seen in Fig.4(a). The local subsonic regions are observed behind the struts and adjacent to the middle wall regions (Fig.4(b)) where static temperature has been found to be more (Fig.4(c)). The comparison of computed top wall pressure distribution with experimental data in the generator along the combustor length at Z/h = 1.6 is shown in Fig.5. Fairly, good match is obtained between computation and experimental measured values except few points. The sudden reduction of wall pressure at X/h =4.7 found in test, could not be explained from the simulation results. The cause of reduction of pressure at X/h = 4.7 in the experimental data, may be due to surface roughness at the measurement point on the wall, or misbehaviour of the pressure transducer in the experiment. At X/h = 6.4 and 11.6, CFD data are found to be more than the experimental value, which may be due to multiple oblique and reflection shocks generated by struts (which is clearly shown in Fig.4(a). Multi-shock structures due to middle wall and struts are clearly visible in the schlieren picture.

Nonreacting Flow with Fuel Injection

To determine the vapourisation and mixing characteristics numerically, liquid fuel is injected through struts in a non-reacting environment and simulations are carried out. Rosin-Rammler diameter of d_e =3 1.31 μm and spray parameter γ =1.5 (equivalent to Sauter mean diameter, SMD =1 1.6 μm) with ϕ = 1.0 are considered in the present study. The static temperature, axial velocity and kerosene vapour mass fraction distribution contour at four struts injection locations (X/h=4.9, 6.4, 8.3 and 10.4) and behind the fourth strut (X/h=11.6) are plotted in Figs.6(i) - (iii) respectively. Kerosene vapour mass fraction is found more in combustor core regions, (Fig.6(iii)) because of the more vaporization of injected fuel due to higher static temperature as visible in the non-reacting flow (Fig.4(c)).

The computed wall static pressure distribution along the flow direction for without/with fuel injection is compared in Fig.7. The wall pressure is almost same for both cases except peak regions (i.e. X/h= 8.3 and 10.4) which may be due to the injection of liquid kerosene, vapourisation and mixing with transverse supersonic airstream. The comparison of average temperature distribution is shown in Fig.8. Static temperature distribution is almost same for both cases within the range of $0 < X/h < 4.8$, after that it is lower in case of with fuel injection compared to without fuel injection case, because, surrounding air medium be-

comes cooler due to the vaporization of liquid kerosene and mixing with incoming air.

The amount of kerosene evaporation along with the fuel injection is plotted in Fig.9 along the length of the combustor. Evaporation of kerosene is defined as the ratio of vapourised kerosene to the total amount of liquid kerosene injected from the struts. It is observed that the amount of liquid kerosene injected from the struts is not completely evaporated within the next immediate strut. Rate of evaporation is more at the vicinity of injection for all the struts. Injected liquid kerosene is seen to be evaporated at $X/h < 18.5$ which is well ahead of the exit of the combustor. The distribution of the mixing efficiency along the length of the combustor is shown in Fig.9 along with fuel injection and vapourisation. The mixing efficiency (η_m) is defined [26] as:

$$\eta_m(x) = \frac{\int_A \alpha \rho_{C12H23} Y_{C12H23} u \, dA}{\dot{m}_{C12H23}(x)}$$

$$\text{with } \alpha = \begin{cases} \frac{1}{\phi} & : \phi \geq 1, \\ 1 & : \phi < 1 \end{cases}$$

Where, ρ_{gas} and Y_{C12H23} are the density and the mass fraction of kerosene vapour in the gas mixture, A is the cross-sectional area and u is the axial velocity. $\varnothing$ is the local equivalence ratio and is defined as:

$$\phi = \frac{1}{2} \frac{M_{o_2}}{M_{C12H23}} \frac{Y_{C12H23}}{Y_{o_2}}$$

Where, M_{C12H23} and M_{o_2} are the molecular weights of kerosene vapour and oxygen respectively, and Y_{o_2} is the mass fraction of oxygen. Even though, the vaporisation is complete well before the exit of the combustor, mixing is not complete within the combustor length. Mixing efficiency increases sharply adjacent to the injection zone and increases slowly in the last divergent portion of the combustor. Maximum mixing efficiency is achieved to 82% at the exit of the combustor.

Reacting Flow Simulation Results : Baseline Case

Reacting flow simulations are carried out for equivalence ratio (ϕ) of 1.0. Mach number, non-dimensionalised static pressure (P/P_o) and static temperature (T/T_o) contour distributions at mid-height of combustor entry plane (i.e. $Y/h = 0.5$) are shown in Fig.10. Mach number is found to decrease while static pressure and temperature are found to increase adjacent to the strut regions, which are due to mixing, combustion and heat release of the kerosene fuel. Mach number is almost fully subsonic behind the struts. In the downstream of the combustor, Mach number is increased and pressure and temperature are reduced, due to expansion of supersonic flow at 7.5° divergent section of combustor. The mass average Mach number, static pressure (P/P_o) and temperature (T/T_o) at the exit of the combustor are 1.79, 0.063 and 1.327 respectively.

Mass average properties i.e. Mach number, static pressure, static temperature and total pressure along the length of the combustor are plotted in Fig.11. Average Mach number is found to reduce from 2.2 at combustor entry to 0.68 at $X/h = 7.6$, due to shock interaction from various walls of the combustor, mixing and combustion of kerosene fuel with vitiated air. In the further downstream of the combustor, Mach number is found to increase due to expansion of flow (shown in Fig.11(a)). Significant subsonic flow pockets are found at fuel injection and combustor intense zones (i.e., X/h = 4.65 m to 10.5) of the combustor. However, the complete cross-section of is not subsonic unlike a ramjet combustor. The flow is not choked through normal shock. In the lower end of scramjet operation ($M_\infty \sim 6.0$), we consider the combustion supersonic if there exists continuous supersonic region along the length of the combustor from entrance to exit. Static pressure and temperature are found to increase at struts region due to combustion of fuel and heat release as shown in Figs.11(b) and (c) respectively. Due to shock interactions and heat release, total pressure decreases along the length of the combustor as shown in Fig.11(d). In the divergent portion of the combustor total pressure remain almost constant. Total pressure availed at the exit of the combustor is 37.3% of the combustor entry value, showing net decrease of 62.7% in the whole scramjet combustor.

Mass fraction of CO_2, O_2 and kerosene vapour at various axial locations are shown in Figs.12 (a), (b) and (c) respectively. Reaction occurs mostly adjacent to the middle wall region of combustor, as observed in Fig.12(a). Considerable amount of O_2 (Fig.12(b)) is found to remain un-burnt adjacent to the side wall regions of the combustor, which is due to the fact that sufficient amount of fuel is not available in these regions which also observed in the non-reacting flow (Fig.6(iii)). Kerosene fuel droplets completely vaporize within the combustor and no liquid droplet was found at the exit of the combustor. Small

amount of un-burnt kerosene fuel vapour has been observed in the core regions adjacent to the middle wall of the combustor (Fig.12(c)). Combustion efficiency (defined as the ratio of the burnt fuel to the total amount of liquid fuel injected from the struts) is calculated to 81.0% at the combustor exit.

Comparison of computed and experimental top wall pressure distributions is shown in Fig.13. Early rise of pressure in the range of $1.1 < X/h < 7.6$ is observed in computed values compared to the experimental results. Computed upstream interaction is more than the experimental results. From the third stage of struts (X/h =7.9) to the downstream, good agreement of the top wall surface pressure is obtained between the computed and experiment values. To find the cause of the difference of the pressure values in the upstream region ($1.1< X/h < 7.6$), number of numerical simulations are carried out with different grids, different spray parameters and different turbulence models.

Effect of Computational Grid

A new grid of size 527 x 77 x 101 (total 4.1 million) was generated and the simulations are carried out using k-ε turbulence model. Increase of grids are mostly provided adjacent to fuel injection struts and near wall regions where flow fields are expected to change more compared to the other regions. Top wall pressure distribution at Z/h=1.6 for two different grids are shown in Fig.14. Almost the same combustor wall pressure with two different grids, demonstrate the grid independence of the results.

Effect of Spray Parameter

Additional numerical simulations are carried out with different values of spray parameters (γ=2.0, 3.0 and 4.0) to find its effect on wall pressure (details of SMD, Rosin-Rammler distribution is given in Table-2). Fuel flow rate was maintained constant in these simulations. Comparison of computed top wall pressure distribution for four spray parameters (i.e. γ = 1.5, 2.0, 3.0, 4.0) along with experimental measured data is shown in Fig.15. It is observed that spray parameter values do not have significant effect on wall pressure.

Effect of Turbulence Models

Three different turbulence models [i.e., k-ε (Case-A), k-ω (Case-B) and *SST*-kω (Case-C)] were studied to assess their predictive capabilities for upstream interaction of the supersonic reactive flow. The qualitative features of the flow field is depicted through the static pressure distributions in the plane passing through Y/h = 0.5 in Fig.16. Upstream interaction (early rise of pressure) is found [Fig.16(a)] to be more in k-ε turbulence model (Case-A) compared to the other two turbulence models. Flow separation zones is also larger in k-ε turbulence adjacent to the side walls due to the interaction of shocks with boundary layer. Comparison of computed top wall pressure distribution for three turbulence models at Z/h = 1.6 along with experimental data is shown in Fig.17. Although the turbulence models show different upstream interaction (different wall pressures in $0.7 < X/h < 8.1$), they predict the same value in the divergent portion of the combustor which produces the maximum thrust for the combustor. *SST*-kω turbulence model (Case-C), has shown better match of top wall pressure distribution with experimental data compared to the other two cases. Comparison of the combustor performance for the three turbulence models in terms of thrust per unit fuel flow rate, combustion efficiency and pressure recovery is provided in Table-3. Since, there is very little divergence in the region where upstream interaction is occurring, the contribution of the increased pressure to thrust is marginal. Maximum deviations for all the parameters are less than 5 %.

Conclusions

To alleviate intermittent / non ignition of kerosene fuel of a flightworthy scramjet combustor at a reduced Mach number and altitude conditions, new wide based fuel injection struts are designed. The new scramjet combustor is numerically explored by performing three dimensional non-reacting and reacting flow simulation using commercial CFD software, CFX-11 to obtain better insight of mixing and combustion process. Three different two equation turbulence models were studied to assess their capabilities in predicting turbulent reacting flows. Single step chemical reaction with Lagrangian Particle Tracking

Table-3 : Comparison of Net Combustor Performance at Exit

Case	Thrust (kgf sec /kg)	Combustion Efficiency (%)	Pressure Recovery (%)
A	781.1	79.0	37.1
B	790.5	80.4	36.3
C	765.7	78.2	38.2

Method is used for combustion of kerosene fuel. Grid independence of the results are demonstrated by performing simulations with two different grids and comparing the results. For non-reacting flow, computed top wall pressures match experimental results extremely well. Although, liquid fuel completely vapourises within the combustor, 82% of kerosene vapour mixes with air stoichiometrically. In case of reacting flow, although top wall pressure matches extremely well in the divergence portion of the combustor, k-ε and k-ω turbulence models predict significant upstream interaction compared to the experimental results. *SST-k-ω* turbulence model predicts the upstream interaction much lower compared to other two models and matches with experimental data in the upstream interaction zone reasonably well. The computed performance parameters with different turbulence models do not vary appreciably with different turbulence models. Variations of spray parameters do not affect the combustor wall pressure significantly.

Acknowledgement

The authors would like to acknowledge the Scramjet Propulsion Team of Directorate of Propulsion, Defence Research and Development Laboratory (DRDL) for providing the combustor configuration and necessary input conditions for the simulation during the course of the work.

References

1. Curran, E. T., "Scramjet Engines: The First Forty Years", Journal of Propulsion and Power, Vol.17, No.6, 2001, pp.1138-1148.

2. Edward, A. K. and Joseph, A. S., "Liquid Jet Injection into a Supersonic Flow", AIAA Journal, Vol.11, No.9, 1973, pp.1223-1224.

3. Northam, G. B. and Anderson, G. Y., "Survey of Supersonic Combustion Ramjet Research at Langley", AIAA Paper 86-0159, 1986.

4. Waltrup, P. J., "Liquid Fueled Supersonic Combustion Ramjets: A Research Perspective of the Past, Present and Future", AIAA Paper 86-0158, 1986.

5. Abbilt, J. D., Hartfiled, R. J. and McDaniel, J. C., "Mole Fraction Imaging of Transverse Injection in a Ducted Supersonic Flow", AIAA Journal, Vol.29, No.3, 1991, pp.431-435.

6. Yokota, K. and Kaji, S., "Two and Three Dimensional Study on Supersonic Flow and Mixing Fields with Hydrogen Injection", AIAA Paper No. 95-6024, 1995.

7. Mitani, T. and Kouchi, T., "Flame Structures and Combustion Efficiency Computed for Mach 6 Scarmjet Engine", Combustion and Flame, Vol.142, No.3, 2005, pp.187-196.

8. Malo-Molina, F. J, Gaitonde, D.V. and Ebrahimi, H.B., "Numerical Investigation of a 3D Chemically Reacting Scramjet Engine at High Altitudes Using JP8-Air Mixtures", AIAA Paper No. 2005-1435, 2005.

9. Rajasekharan, A. and Babu, V., "Evaluation of a Ramp Cavity Based Concept Supersonic Combustor Using CFD", Progress in Computational Fluid Dynamics, Vol.9, No.1, 2009, pp.16-29.

10. Behera, R. and Chakraborty, D., "Numerical Simulation of Combustion in Kerosene Fueled Ramp Cavity Based Scramjet Combustor", Journal of Aerospace Sciences and Technologies, Vol. 58, No. 2, 2006, pp.104-111.

11. Dufour, E. and Bouchez, M., "Computational Analysis of a Kerosene Fuelled Scramjet", AIAA Paper, 2001-1817, 2001.

12. Manna, P., Behera, R. and Chakraborty, D., "Liquid Fueled Strut Based Scramjet Combustor Design - A CFD Approach", Journal of Propulsion and Power, 24(2), 2008, pp.274-281.

13. Javed, A. and Chakraborty, D., "Numerical Simulation of Supersonic Combustion of Pylon Injected Hydrogen Fuel in Scramjet Combustor", Journal of the Institution of Engineers (India), 87, 2006, pp.1-6.

14. Pannerselvam, S., Thiagarajan, V., Ganesh Anavardham, T. K., Geetha, J. J., Ramanujachari, V. and Prahlada., "Airframe Integrated Scramjet Design and Performance Analysis", ISABE Paper 2005-1280, 2005.

15. Chandrasekhar, C., Tripathi, D. K., Ramanujachari,V. and Panneerselvam, S., "Experimental Investigation of Strut Based Supersonic Combustor Burning Hydrocarbon Fuel", XVIII ISABE, Beijing, China, September, 2007.

16. Ramanujachari, V., Chandrasekhar, C., Satya, V. and Panneerselvam, S., "Experimental Investigations of a Strut Based Scramjet Combustor Using Kerosene Fuel", 7th Asia-Pacific Conference on Combustion, National Taiwan University, Taipei, Taiwan, May, 2009.

17. Manna, P., Dharavath, M., Sinha, P.K. and Chakraborty, D., "Optimization of a Flight-worthy Scramjet Combustor Through CFD", Aerospace Science and Technology, Vol.27, 2013, pp.138-146.

18. Malsur Dharavath, Ranjith, A.R., Manoj, R., Manna, P. and Debasis Chakraborty., "Effect of Turbulence Models on Scramjet Combustor Performance with Kerosene Fuel", Paper No. CP-04, 16th Aeronautical Society of India, CFD Symposium, August,12-13, Banglare, 2014.

19. ANSYS-CFD, Release 11.0: "Installation and Overview", 7th July, 2007.

20. Launder, B.E. and Spalding, D.B., "The Numerical Computation of Turbulent Flows", Computational Method in Applied Mechanical Engineering, Vol.3, 1974, pp.269-289.

21. Wilcox, D.C., "Multiscale Model for Turbulent Flows", AIAA Journal, Vol.26, No.11, 1988, pp.1311-1320.

22. Menter, F.R., "Two-Equation Eddy-Viscosity Turbulence Models for Engineering Applications", AIAA Journal, Vol.32, No. 8, 1994, pp.1598-1605.

23. Lefebvre, A.H., "Atomization and Sprays", Hemisphere publishing Corporation, Bristol, First edition, 1989.

24. Ramanujachari, V., "Spray Parameters for Different Equivalence Ratios", Private Communication.

25. ANSYS ICEM-CFD-11, "Installation and Overview", January, 2007.

26. Shuhei, T., Kazunori, W., Sadatake, T., Mitsuhiro, T. and Michikata, K., "Effects of Combustion on Flowfield in a Model Scramjet Combustor", Twenty Seventh Symposium (International) on Combustion, The Combustion Institute, 1988, pp.2143-2150.

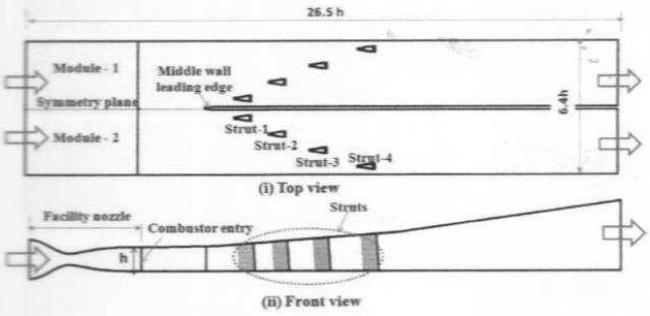

Fig.1a Scranjet Combustor with Facility Nozzle

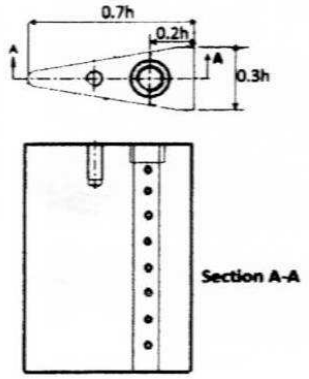

Fig.1b Schematic Picture of Strut

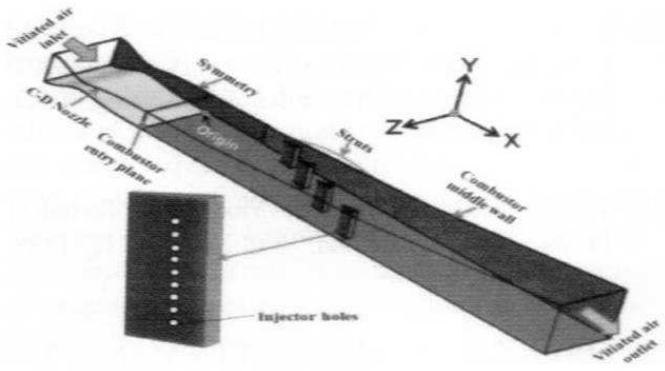

Fig.2 Computational Domain

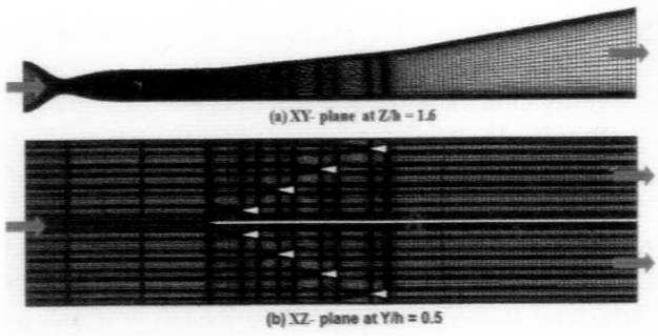

Fig.3 Grid Distribution on Various Plane (2.6 Million)

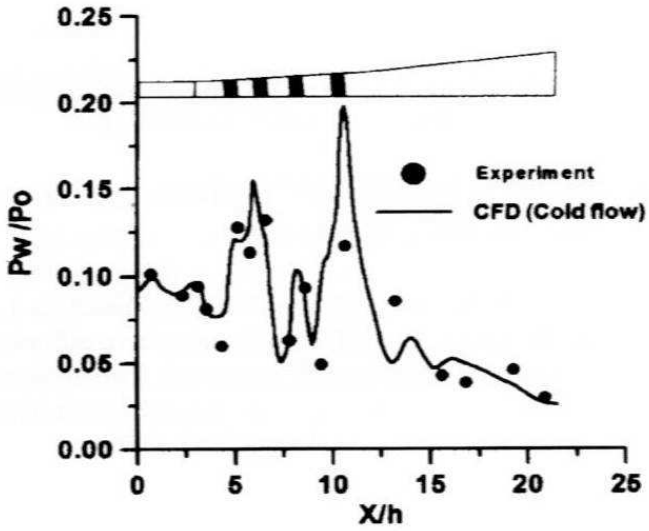

Fig.5 Comparison of Top Wall Pressure

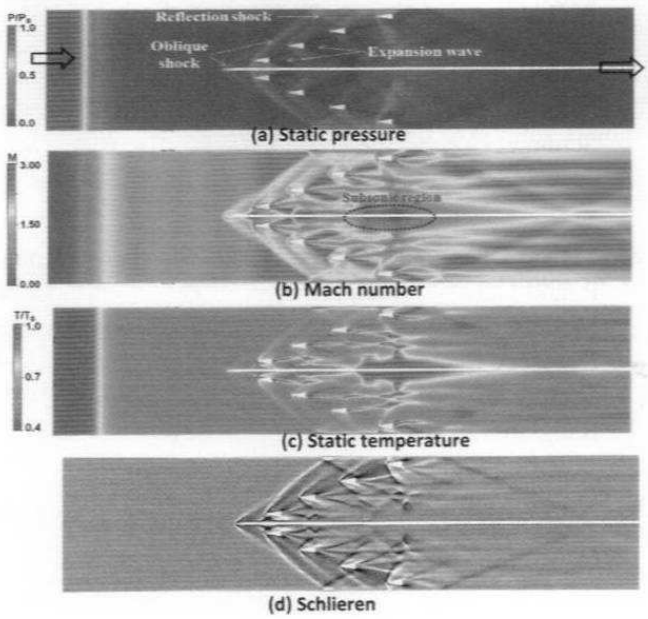

Fig.4 Composite Flow Field on Plane Passing Through Y/h=0.5 (a) Static Pressure (b) Mach Number (c) Static Temperature (d) Schlieren

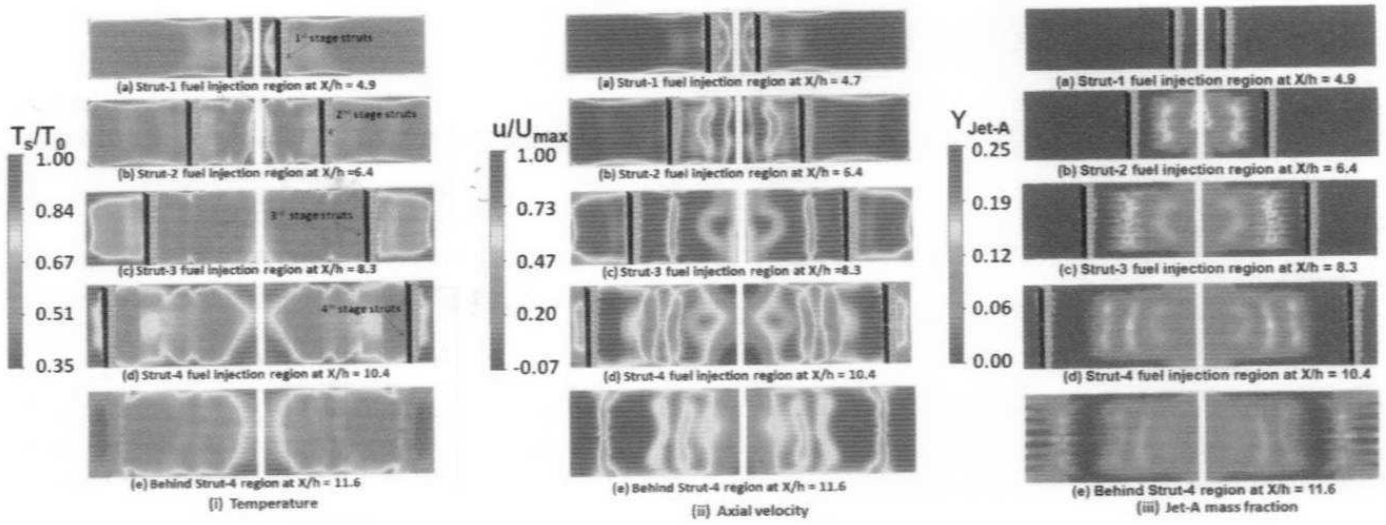

Fig.6 Flow Properties at Different Axial Locations (x/h=4.9, 6.4, 8.3, 10.4 and 11.6) (i) Temperature (ii) Axial Velocity (iii) Jet-A Mass Fraction

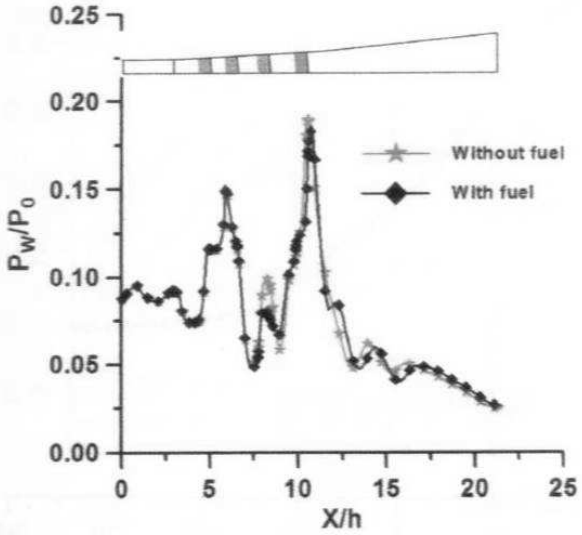

Fig.7 Comparison of Wall Pressure

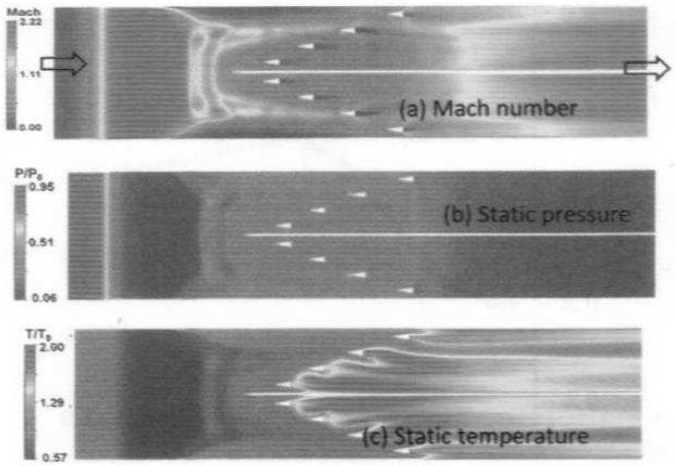

Fig.10 Contours of (a) Mach Number (b) Static Pressure and (c) Static Temperature at Mid-Height of Combustor Entry at Y/h = 0.5

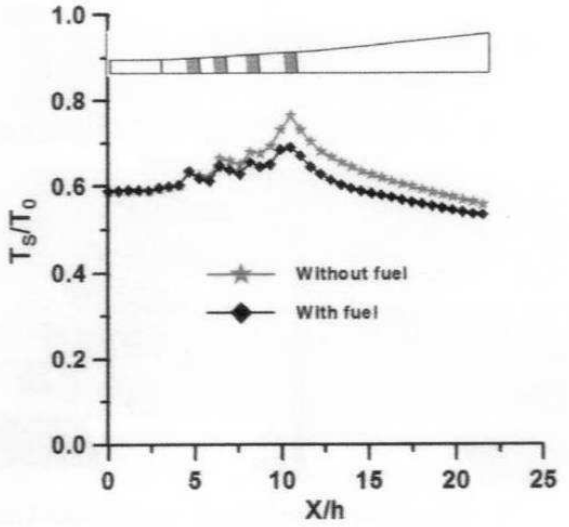

Fig.8 Comparison of Average Temperature

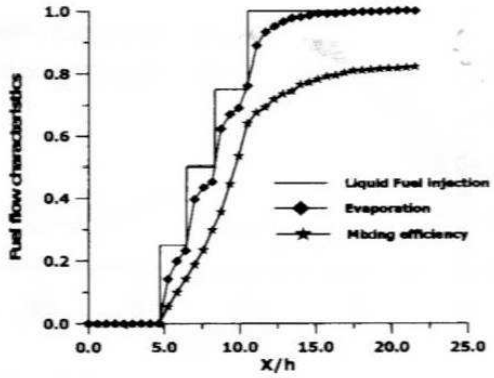

Fig.9 Liquid Kerosene Evaporation and Mixing Characteristics of the Combustor

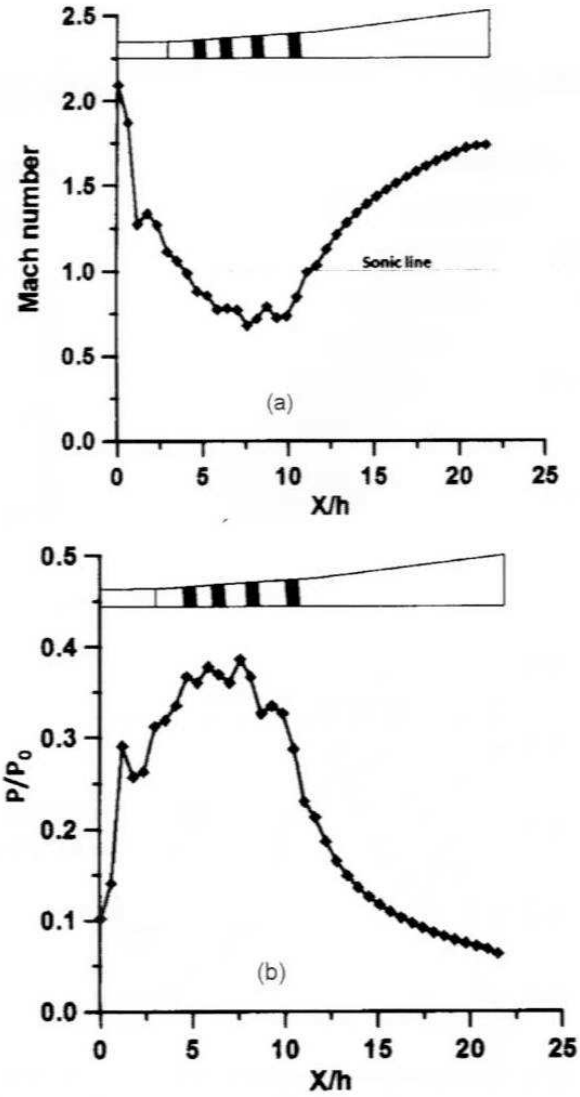

Fig.11 Average Property Distribution Along the Combustor Length (a) Mach Number (b) Static Pressure

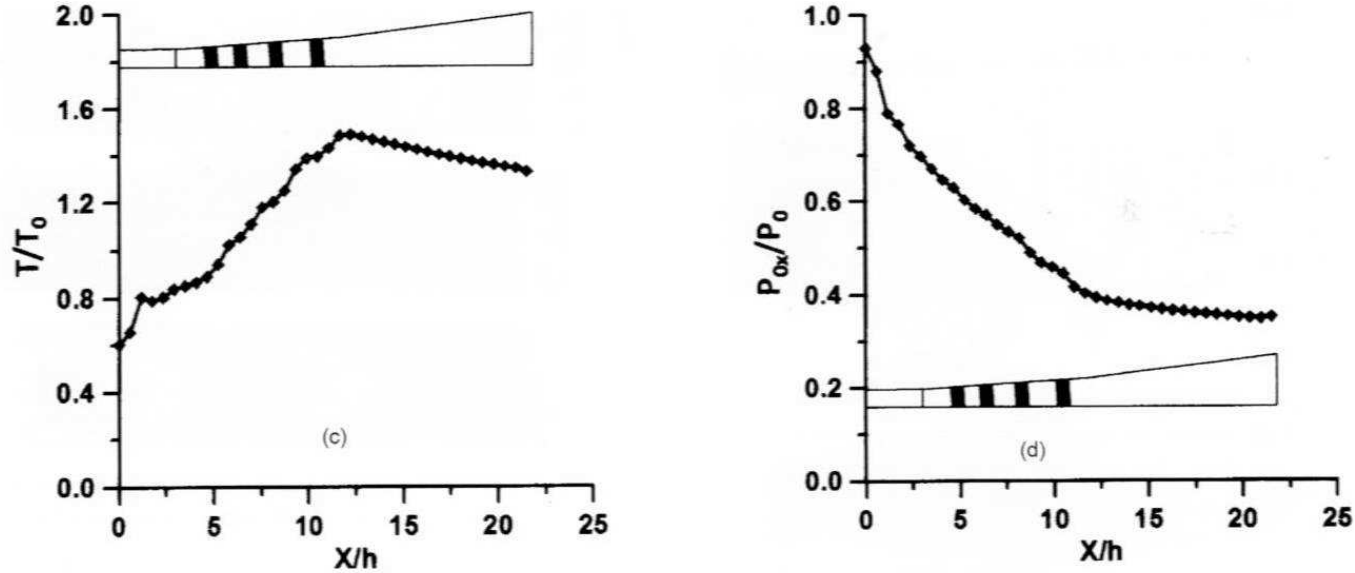

Fig.11 Average Property Distribution Along the Combustor Length (c) Static Temperature and (d) Total Pressure

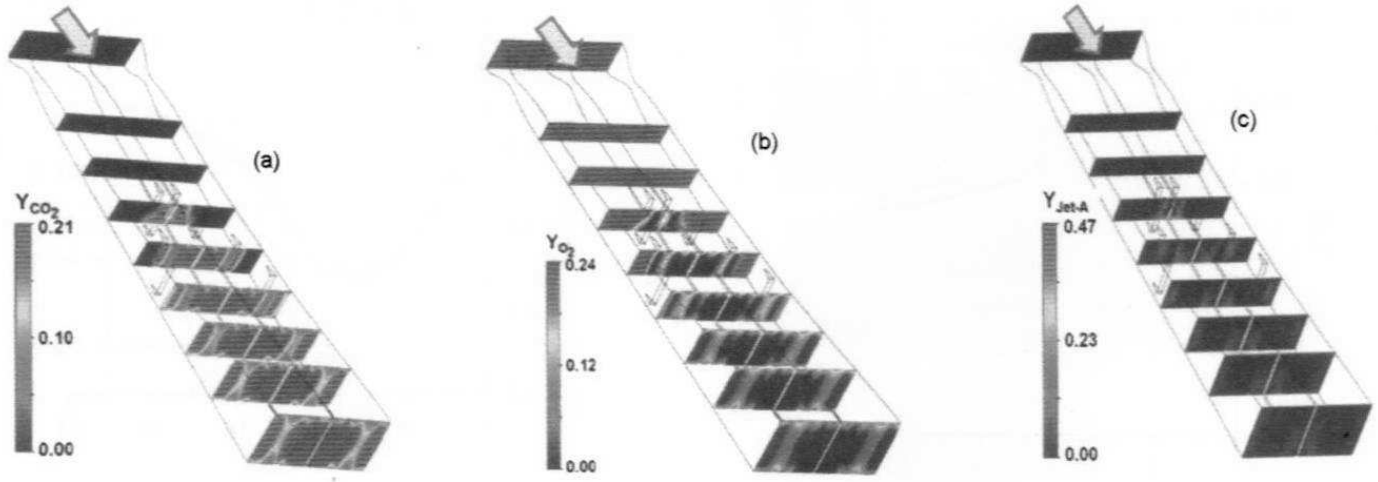

Fig.12 Distributions of (a) CO_2 Mass Fraction, (b) O_2 Mass Fraction and (c) Kerosene Vapor Mass Fraction at Various Axial Locations (x/h = -5.02, 0.0, 2.91, 5.81, 8.72, 11.63, 14.53, 17.44 and 21.51)

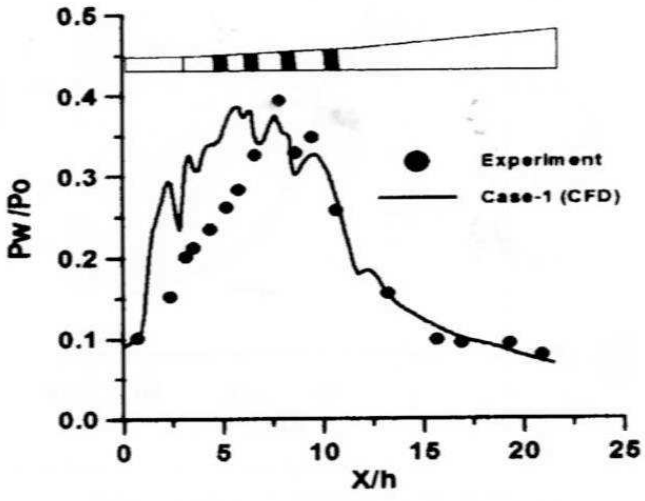

Fig.13 Comparison of Wall Pressure with Experiment Data

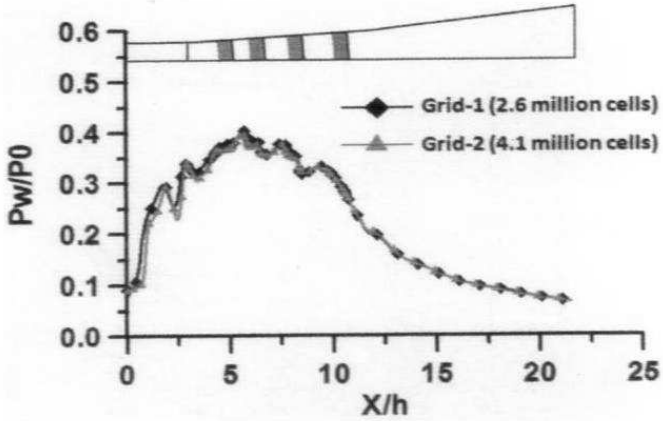

Fig.14 Comparison of Top Wall Pressure with Two Different Grids for k-ε Turbulence Model

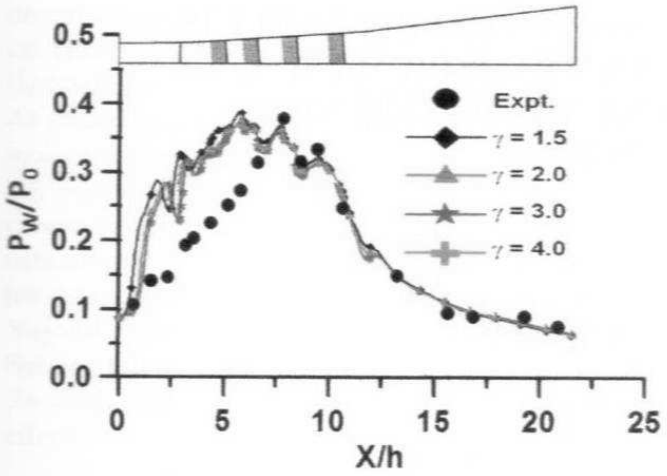

Fig.15 Comparison of Wall Pressure with Different Spray Parameter

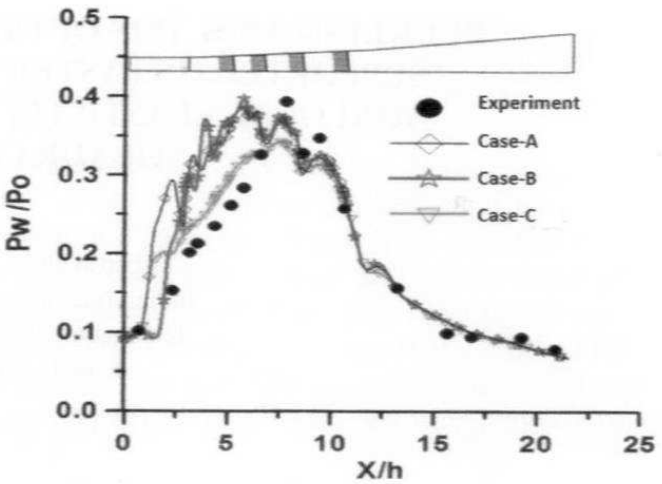

Fig.17 Comparison of Top Wall Pressure Distribution

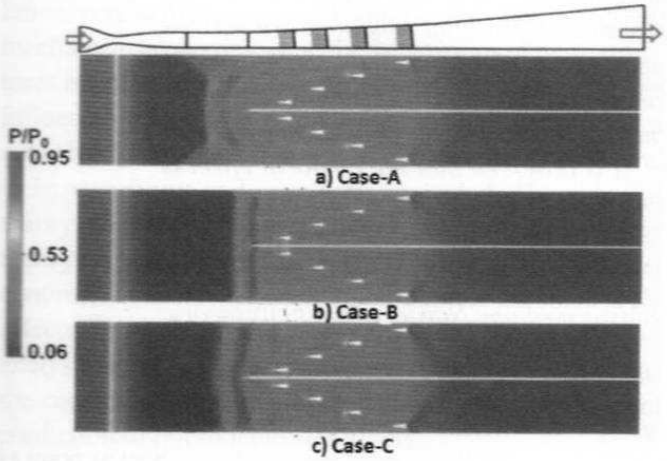

Fig.16 Comparison of Pressure Contour at Y/h = 0.5
(a) k-ε Model (b) k-ω Model (c) SST k-ω Model